Light scattering microscope as a tool to investigate scattering heterogeneity in tissue

Alois K. Popp*[a], Megan T. Valentine[a], Peter D. Kaplan[b], David A. Weitz[a]

[a] DEAS and Physics Department, Harvard University, Cambridge, MA, 02138
[b] Unilever Research U.S., Edgewater, NJ, 07020

ABSTRACT

Rayleigh light scattering has not yet been used for quantitative investigations of heterogeneous systems. Preconditions for such an experiment are a well defined scattering geometry and independent information about the local state of the sample. We have designed a new instrument that meets these criteria: a light- scattering microscope with simultaneous imaging. We demonstrate the ability to characterize local differences within one tissue type as well as global differences between tissue types. Real space images of the sample are taken by normal video microscopy techniques. The light scattering pattern is analyzed by the evaluation of wave- vector dependence (form factor) and scattering direction of the scattered intensity. Statistical analysis of scattering patterns show what is important for the characterization and classification of tissues and heterogeneous structures. Real space images provide context for scattering analysis. The light scattering microscope is a powerful tool for characterization of local structural order in inhomogeneous structures like tissues.

Keywords: Rayleigh light scattering, tissue optics, static light scattering, microscopy, heterogeneities

1. INTRODUCTION

In the pursuit of non-invasive measures of physiology and structure, the field of tissue optics has been growing rapidly in the 1990s. Many applications of tissue optics rely on differences in light scattering and absorption between different tissue types, such as tumor and non- tumor [1, 2]. Focussed on understanding these differences, a significant literature has appeared on the origin of light scattering in tissue [3, 4] (and references therein).

Researchers have primarily taken three different experimental approaches:

(1) Photon transport measurements of tissue [3, 5-11] or tissue phantoms [12-15], using various experimental geometries. Bulk tissue is best described as turbid media. Transport measurements focus on measuring bulk quantities like absorption, transmission or reflection coefficients. The values of these coefficients vary due to the physiological conditions of the sample as well as due to species- specific variability and differences in the techniques [2, 16].

(2) Averaged scattering experiments from dilute suspensions of cells and organelles to find the structures that are the main contributors to the light scattering from tissue [17-20]. It has been tried to relate the also measured optical properties of the tissues to the scattering from constituent organelles [17].

(3) Scattering measurement from excised tissue. Up to now, most of these investigations focussed on measuring average tissue scattering properties from mounted slices [21, 22], using tissue slices of thicknesses between 100 and 1000 μm.

Furthermore, various models have been developed for these approaches to describe the experimental results from transport measurements [3, 23-25] and light scattering from cells and cell suspensions theoretically [26, 27].

This report is a novel example of the third approach. Working with thinner excised tissue slices (20 μm), we performed simultaneous microscopic imaging and scattering measurements of numerous small regions. The report discusses the technique, the differences between tissues and analyzes both the aggregate and individual statistical properties of scattering patterns with an eye towards describing the microscopic origins of light scattering in tissue. The principal result is that extra- and super-cellular tissue organization is responsible for a large fraction of the most distinctive qualitative features of scattering patterns.

We study the optical properties of thin unstained tissue slices with a newly designed light scattering microscope [28].

* Correspondence: Email: alpopp@deas.harvard.edu; Telephone: 617 496 8049; Fax: 617 496 3088

In *Optical Biopsy III*, Robert R. Alfano, Editor,
Proceedings of SPIE Vol. 3917 (2000) • 1605-7422/00/$15.00

This microscope-based light-scattering apparatus allows us to both observe real space images and simultaneously perform static light scattering measurements. By using a collimated beam in the sample plane and imaging the sample simultaneously, we can select the scattering volume of interest and control the size and placement of the beam. The scattered light is imaged onto a CCD-detector. Previous attempts to use the microscope as a scattering platform either used a highly divergent beam in the sample plane which made interpreting static light scattering difficult [29-31], or did not include imaging [32] which provides an intuitive if not always formal tool to help unravel scattering patterns.

The beam is not larger than 70 μm in diameter. Therefore, we can directly relate scattering to the structures the light is scattered from by imaging on a lengthscale at which heterogeneities in the tissue can be resolved. Without a traditional, image based view of heterogeneities we see no way to understand the connection between scattering patterns and tissue structure. Little is known about how variations in tissue organization and strucuture contribute to light scattering in tissue. We do know that tissues show specific heterogeneities of sizes and organization. Hair, pores, sweat glands, epithelial layers, collagen fibers, lung alveoli, bile ducts and capillaries are only a few examples.

The data from light scattering experiment consists of the two-dimensional intensity distribution of the scattered light, which we can relate to the scattering angle by a simple calibration procedure and derive both the azimuthal averaged and fully anisotropic static form factor from the intensity distribution. These patterns are analyzed with statistical methods. But we can use the real space images to check on which structures the light is scattered from, a uniquely useful feature. We have successfully applied our technique to investigate heterogeneities inside different tissue types and are able to measure differences between tissue types due to the presence of specific heterogeneous structures. A tissue consisting of a well organized structure like striated muscle has a unique scattering pattern showing strong anisotropy in scattering.

2. EXPERIMENTAL METHODS

2.1. Design of the static scattering microscope

By using a commercially available inverted microscope (Leica DM-IRBE) with additional custom-made optical and mechanical components as shown in Figure 1, we perform simultaneous scattering measurements and imaging. A laser beam (Coherent Innova 304, 514.5 nm) is launched from a fiber optic coupler that is mechanically mounted to an extension of the microscope above the condenser. A series of neutral density filters and a linear polarizer attenuates the laser intensity to typically less than 50μW. A beamsplitting cube splits the laser intensity into two paths of equal intensity (accomplished by rotation of a linear polarizer). One path leads directly to a photodiode that monitors the input laser intensity, the other beam is coupled into the light path of the microscope by a dichroic mirror. It scatters from the sample and is collected at the detector. On the collection side of the sample, the objective lens of the microscope (plan-apochromatic, 100x magnification) with high numerical aperture (N.A.=1.4) collects both scattered light and unscattered transmitted beam. By using index-matching immersion oil to eliminate the air-glass interfaces at the condenser and objective, we can collect scattered photons up to an angle close to 90 degrees from aqueous samples. In the back focal plane of the objective (BFPO), all parallel rays are brought to a point. By collecting light in this plane, we collect photons through the same scattering angle, θ. In the BFPO, the scattering angle depends only on the distance between the collection point and the center of the BFPO, $\delta x \sim \sin\theta$. In most objectives, the BFPO is inconveniently located just inside the objective's exit pupil. We built a projection system to re-image the BFPO in a more accessible plane above the internal housing of the microscope, through a phase telescope mounted on the camera port of the trinocular head. In the projected BFPO, we place a beamblock to remove the unscattered transmitted light. The beamblock consists of a 1mm diameter metal rod. The beamblock obscures light scattered at angles less than 3 degrees. One final relay lens re-images the scattering plane and beamblock, onto a 16 bit cooled CCD detector (Princeton Instruments, Model CCD-512SF) with a 512x512 array of 24μm square pixels. The intensity at each pixel can be measured using a variety of exposure times to increase dynamic range.

The incident laser beam is focussed to a point on the back focal plane (BFP) of the condenser, ensuring a collimated beam in the sample plane. With our design, a 1mm diameter laser beam forms a spot of 40 microns with a divergence angle of less than 10 mrad. We can increase or decrease the illuminated spot size with the addition of an enlarging or reducing telescope before the focussing lens at the field iris. Additionally, samples can be imaged via conventional bright-field microscopy by diverting a portion of the illuminating light to the side camera port, where a 8 bit CCD camera can record the real space images. We place a filter before the camera to block out the transmitted and scattered laser beam, and allow only the red portion of the illuminating halogen source to pass. This allows us to record both the real space image from the brightfield microscopy and the corresponding Fourier space image from the static light scattering. We perform several calibrations for the CCD detector, namely correcting for read-out noise, thermal noise, offset and pixel to pixel variations due to the quantum efficiency and area of each pixel by taking several pictures of a dark background and a uniformly illuminated ("flat") background. There is a final correction for flare at low angles. Flare is measured by scattering from an empty or solvent

filled sample chamber to find the amount of stray light. This flare intensity is then subtracted from the experimental data using an appropriate scaling factor to reflect the differences in input laser intensity between the two images. An attenuation factor is also used to compensate for the attenuation of the beam by the sample compared to the empty sample chamber. These corrections are typically small compared to the scattering intensity at even fairly large angles.

2.2. Raw data conversion and data analysis

On the CCD detector, we collect the intensity as a function of the radial distance of the scattered light towards the unscattered beam. To convert this distance- dependent function into a wave- vector dependence ('form factor'), we have to relate the radial distance to the wave vector of the beam and find the proportionality factor between them. We know that the radial distance of the scattered light on the BFPO (and therefore on the CCD detector) is proportional to the sine of the scattering angle: $\delta x \sim \sin\theta$. The (sample dependent) proportionality constant can be found by scattering from an object showing a calculable scattering pattern. We used a graticule for this calibration: Calculating the scattering angles of maxima and minima from the known distances of the gridlines (d) using Bragg's law and measuring the appropriate positions of maxima and minima on the CCD detector (δx), we can calculate the conversion factor C:

$$\sin\theta_G = \frac{m*\lambda}{d} = C*\delta x, \tag{1}$$

with λ being the wavelength of the laser beam and m the order of the maximum.
Using Snells law, we can apply this conversion to any sample S with known refractive index n_S:

$$\sin\theta_S = \frac{n_G}{n_S} * \sin\theta_G \tag{2}$$

Once the conversion from the distances into scattering angles is known, we can calculate the scattering wave vector $q = 4\pi n \sin(\theta/2)/\lambda$, where n is the index of refraction of the sample, and λ is the wavelength of the incident beam. In our data analysis, we have divided our scattering patterns into concentric rings of fixed wave– vector around the beam- center and have calculated the average intensity of each of all pixels inside the ring. Results are shown in section 3.
To present a picture of the measured sample which is as close to the average and to investigate the content, to which heterogeneities contribute to the average appearance of the sample, we have taken between 25 and 35 images and measurements of randomly selected spots on the sample. Furthermore, we have screened regions containing interesting heterogeneities to investigate the change in scattering from homogenous tissue to the heterogeneity. The measured and corrected scattering patterns have been converted into form factors. Additionally to that, anisotropy in the scattering patterns has been determined by calculating average intensities on a radial grid. The angular regions between 0° and 10° and between 350° and 360°, which were covered by the beam- block, have not been taken into account. In both cases the averaged intensities have been divided by the exposure time and the intensity of the incoming laser beam to allow comparison of measurements taken with different values of these parameters.

2.3. Sample processing

We have tried to keep the sample processing technique as simple as possible to prevent further artifacts due to sample processing [3]. Lung, skin and muscle have been directly frozen and stored in liquid nitrogen or a –70C freezer until the slicing procedure. The Xenopus Sartorius muscle and has been stored, sectioned and processed like the porcine samples. The frozen tissue samples were sectioned 20 microns thick, using a standard cryomicrotome. The slices were directly transferred from the knife to a small coverslip (18 mm x 18 mm), which was glued onto a microslide, using ultravacuum grease to seal the sample airtight. The samples were stored for 2 weeks at –20°C or at 4°C overnight, if measured the next day.

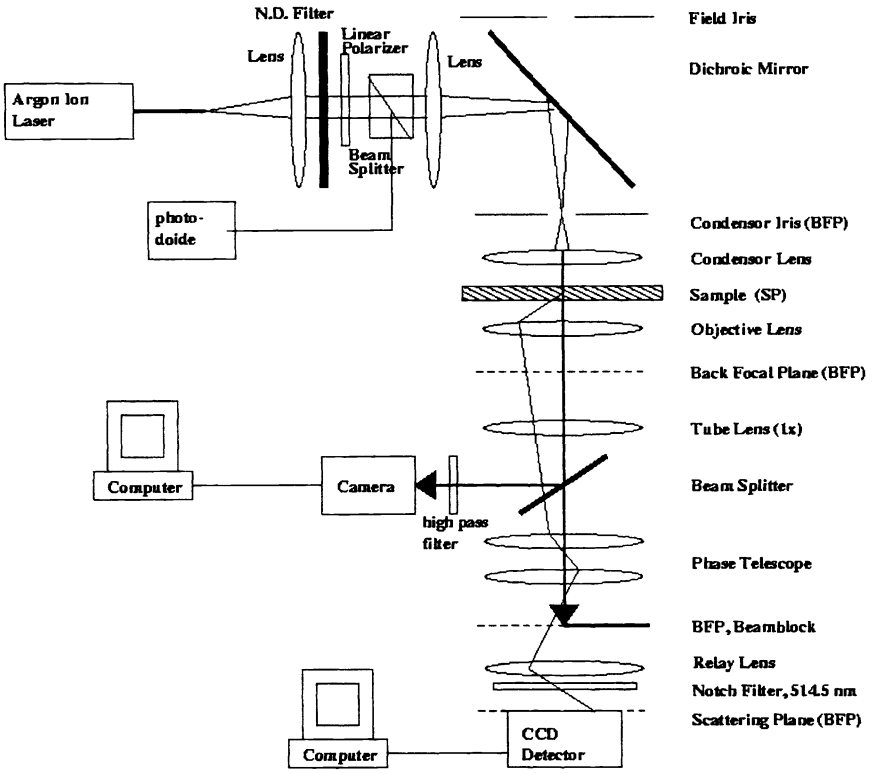

Fig. 1. Opto-mechanical design of the light scattering microscope.

3. RESULTS

3.1. Scattering from muscle

The aim for this study was to use a well defined sample to compare visible and well understood structure, striated muscle, to scattered intensity patterns. In comparison to that, samples consisting of muscle fibers from more randomly, but predominantly crossectionally oriented muscle have been measured. The obvious differences between orientations should be obvious in the scattering pattern. This represents a first step towards working on less obviously distinguishable tissues.
Striated muscles are a well described system[33]. The tissue is highly ordered, containing elongated cells enriched in actin- and myosin filaments giving the muscle its characteristic polar structure. We prepare longitudinal sections from precisely excised Xenopus Sartorius muscle and Porcine leg muscle. The randomly sectioned porcine muscle shows no directionality. The fiber bundles are randomly oriented, often perpendicular to the surface. In our approach to relate scattering from small, well defined spots of a size comparable to that of a muscle fiber bundle to the structure and morphology of the tissue, we took more than 30 single measurements of two slices of both tissues. Examples, real space images together with the scattering patterns, are shown in Fig.2. A comparison of the scattering images of Fig. 2 by eye shows the influence of orientation: The scattering pattern of the Xenopus Sartorius muscle has a preferred direction of scattering, whereas the porcine muscle tissue shows a relatively isotropic pattern. We calculated the form factor and directional analysis as described in the section 2.2., taking a value of 1.41 for the refractive index of muscle from the literature [2]. Not surprisingly, the pronounced difference in scattering patterns does not survive the process of azimuthal averaging - both tissue types obey the same power law, showing

no difference in decay between the highly ordered and the unordered muscle sample (Fig. 3, upper graph). This behavior has also been observed after averaging over all measurements (Fig 6). Differences in form factors have been found in terms of the total scattered intensity and the fine structure of the form factor of the Sartorius muscle. The observed differences in total scattered intensity can be due to a number of effects and need not be the result of differences in tissue organization, as discussed in [2, 3]. The differences in the anisotropy of the scattering pattern, however, are due to differences in tissue organization.

While, without azimuthal sensitivity, we find little to separate the two muscles, the directional analysis found striking differences between the well ordered Sartorius muscle and the porcine leg (Fig. 3, upper graph). Repeated rotation of the sample resulted in a change of the orientation of the fibers and therefore in the orientation of the streak- like feature seen in the scattering pattern, as shown in the directional analysis of three consecutive measurements after rotation of the sample (Fig.3, lower graph). With this experiment, we have shown that we can directly relate scattering pattern and microscopic image in the case of ordered tissue structures like muscle fibers oriented parallel to the surface of the coverslip. A detailed analysis of the preferred scattering direction showed maxima and minima in intensity along the streak-like features of the intensity distribution. They are also the reason for the fine-structure of the form factor of this sample. These need to be analyzed in detail, because they might be the contribution of cellular and sub- cellular components to the scattering, like previous experiments in backscattering geometry have shown [34]. Having understood the fine- structure, we might be able to relate our findings to tissue types that don't show a pronounced scattering in one direction. The ultimate aim is to use our knowledge about the origin of these features to explain the contribution from cellular components to scattering for other tissue types as well.

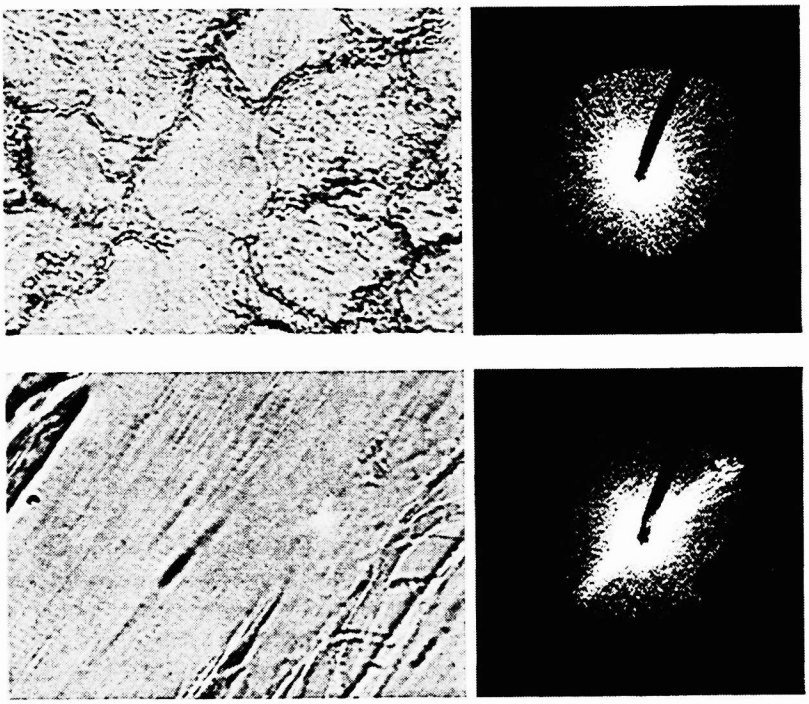

Figure 2: Real space images (left) and scattering patterns (right) from different muscular tissues. On the upper half, predominantly crossectional oriented fibers from a porcine leg muscle are shown. In the lower half, Xenopus Sartorius muscle with fibers oriented parallel to the surface of the coverslip can be seen. The real space images show a field of view of 60 μm length. The scattering patterns are intensity distributions and show bright spots at high scattered intensity. Images show the surface the incident laser beam is directed to.

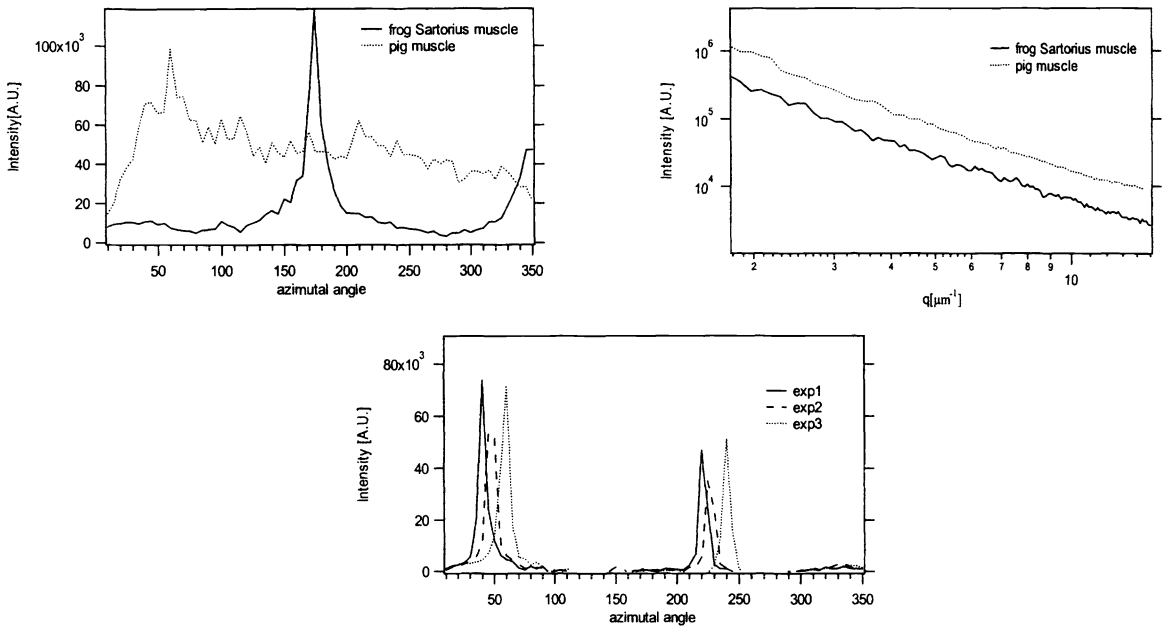

Figure 3: Directional analysis (upper right graph) and form factor analysis (upper left graph) of measurements from porcine muscle and Xenopus Sartorius muscle. Rotating the Sartorius muscle sample rotates the scattering pattern (lower graph).

3.2. Investigation of heterogeneities

Unlike muscle, many tissue types are inhomogeneous. Many organs consist of more than one tissue type, often showing super- cellular structures typical and functionally important for the organ. Some tissues like skin show structures consisting of a- cellular biological matter. Dermal tissue, for example, consists mainly of keratin fibers. Structures inside the skin like pores, sweat glands and hair lead to the idea that these heterogeneities contribute to measured average quantities in an important way. Furthermore, the stratum corneum shows a complex surface topology on a microscopic length scale, which contributes to the appearance of skin. As an example, we concentrate on the measurement of a small, well defined heterogeneity like a hair. Hairs in the tissue are surrounded by dense accumulations of fibrous connective tissue belonging to the dermis. A thickened basal lamina, the glassy membrane, separates the dermis from the epithelium of the hair follicle. The outer layers of follicular epithelium form at the external root sheath, followed by the internal root sheath and the cortex of the hair. As the material properties of tissue and hair (e.g. scatterer density, refractive index) that contribute to light scattering are different from one image to another, a prominent change in scattering patterns can be expected. We have performed our measurements in a scanning mode, probing the region containing a hair in a horizontally sectioned dermal slice of porcine skin. We took several measurements between regions of homogeneous tissue and the center of the hair. Here, the observed scattering patterns changes, when the hair is approximated, from an isotropic to a highly anisotropic scattering pattern. In the experiments with skin, the decay of the form factor does change with position in the tissue (Fig. 5). While approaching the root sheaths, the single form factors show a slower decay. It seems, however, that under certain conditions the form factor can be used to describe differences between tissues and heterogeneities present therein. A possible explanation for this effect is given in section 3.3., as this behavior of the form factor is also valid for averages of form factors.

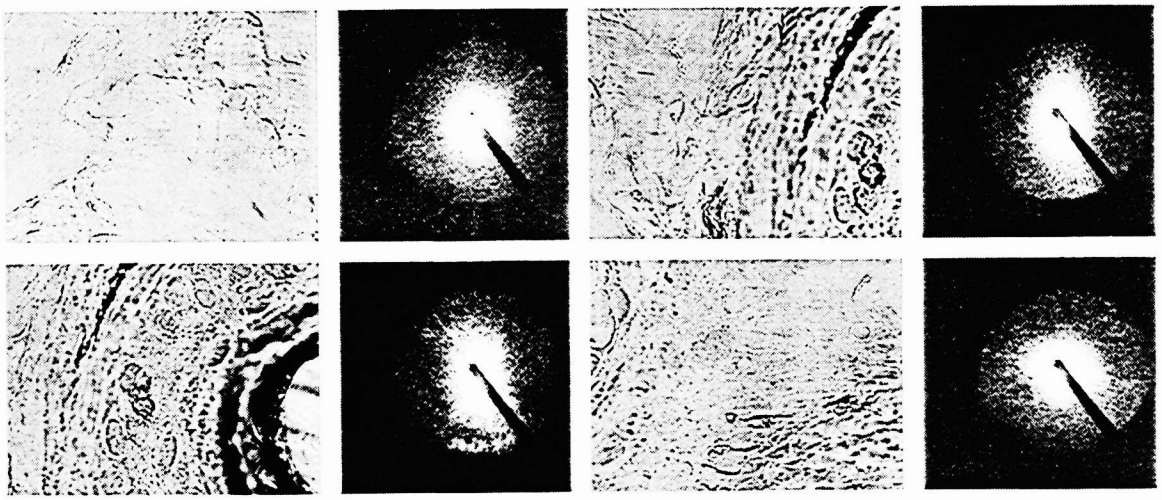

Fig 4: Scattering from skin in a scanning mode. Scattering images and real space images of a selection of experiments are shown. From upper left to lower right: Dermal tissue (experiment 25), approaching external root sheath (exp 33), approaching an internal root sheath (exp. 38), scattering from inhomogeneous tissue away from the hair. The form factors of each of these measurements are shown in Fig 5.

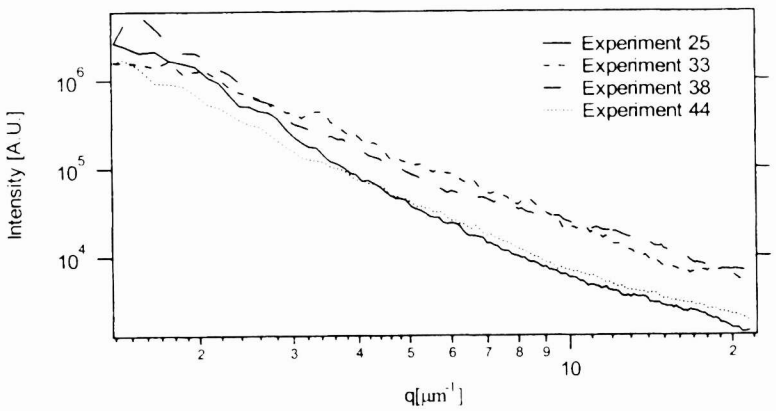

Figure 5: The decay of the form factors shows differences between tissue from the dermis (Experiments 25 and 44) and the heterogeneous region close to a hair (Experiments 33 and 38): The form factors of measurements approaching the external (Exp.33) or internal root sheath (Exp. 38) decay slower.

3.3 Averaging single measurements

To express the average optical properties of our samples, calculated as averaged form factor and anisotropy, we have simply added up the single form factors and anisotropies of every measurement and divided by the number of measurements. Averaging smoothes the fine structural features of single measurements and leads to a simpler description of the optical properties of a sample. Form factors calculated from raw data of single measurements often cannot be fitted to a power law. However, these averaged properties still contain the measured heterogeneities. Whenever heterogeneities are present, their optical properties contribute also to the average. Having measured several horizontally sectioned samples of porcine skin in various depths, we have calculated a simple average of the form factors for each slice. These average form factors have been fitted to the power law for the wave- vector dependence q^{χ} in a dynamic range between $q = 2.7$ and $11.9\mu m^{-1}$. For better comparison, the form factors have been normalized to the first point of the power law fit (Fig. 6). The value of the power

exponent x for all our skin samples ranged between –3.2 and -3.7. Using an application of the theory of fractal dimensions to light scattering, the power law coefficient can be described in terms of fractal dimension: $x = 6 - D_f$. This law expresses our results in fractal dimensions. For all porcine skin samples, D_f reached values between 2.3 and 2.8. A D_f. between 2 and 3 is unique for randomly oriented surfaces [35]. Rayleigh scattering (Intensity ~ q^{-4}) for example, can be explained to be scattering from perfectly smooth random surfaces. D_f increases towards 3 with increasing roughness of the surface. Microscopic imaging of our skin samples showed a relatively heterogeneous surface, especially in the epidermal layer. All other tissues showed a much slower decay coefficient x being about –2.5 (Fig. 7). We assume that the decay of the form factor of skin tissue is mostly due to scattering from surfaces. With the approach of the fractal dimension, one could also explain the slower decay of the single form factors of the tissue measurements (Fig.5) by taking into account the complex surface topology around the hair. In other tissues, the substructure seems to be much more important. We are fully aware of the fact, that the fractal dimension approach includes the danger to oversimplify the complex material properties of tissue and heterogeneities which are probed by our scattering technique. For example, the nature of the material the light is scattered from, is not explained by this approach.

We have already shown that a form factor is not always the appropriate measure for the optical properties of tissue and that other forms of analysis like a calculation of the preferred scattering direction have to be used to investigate the optical properties of tissue precisely. Furthermore, more elaborate statistics tools have to be used in the future for our approach, as we are dealing with numerous measurements. Mean and standard deviation as well as the analysis with higher moments (data not shown) have already been shown to be useful to describe the differences in scattering directions. With the help of Fourier analysis, one might be able to compare the radial shape of single scattering patterns. Another approach to the analysis might include pattern recognition tools.

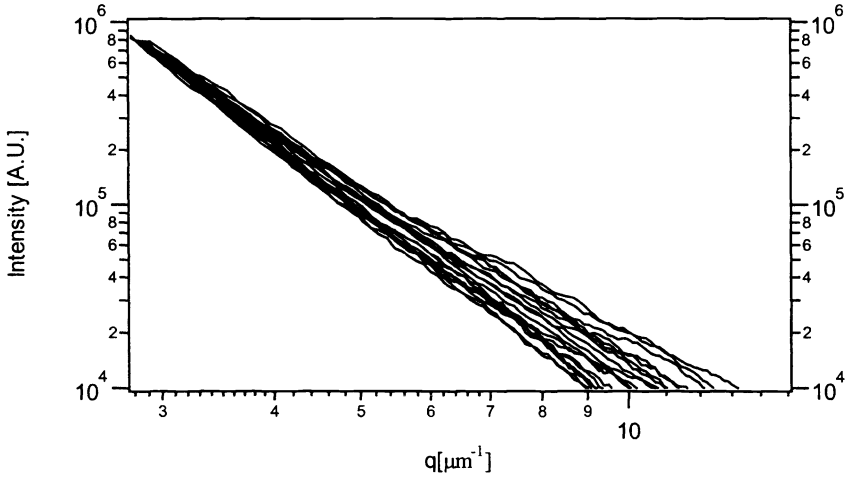

Figure 6: The azimuthally and spatially averaged form factors of 18 slices of porcine skin, normalized to the first point used for fitting. The decay can be fitted to a power law and has been found to result in a fractal dimension between 2.3 and 2.7, which could be interpreted as scattering from randomly oriented surfaces of different roughness.

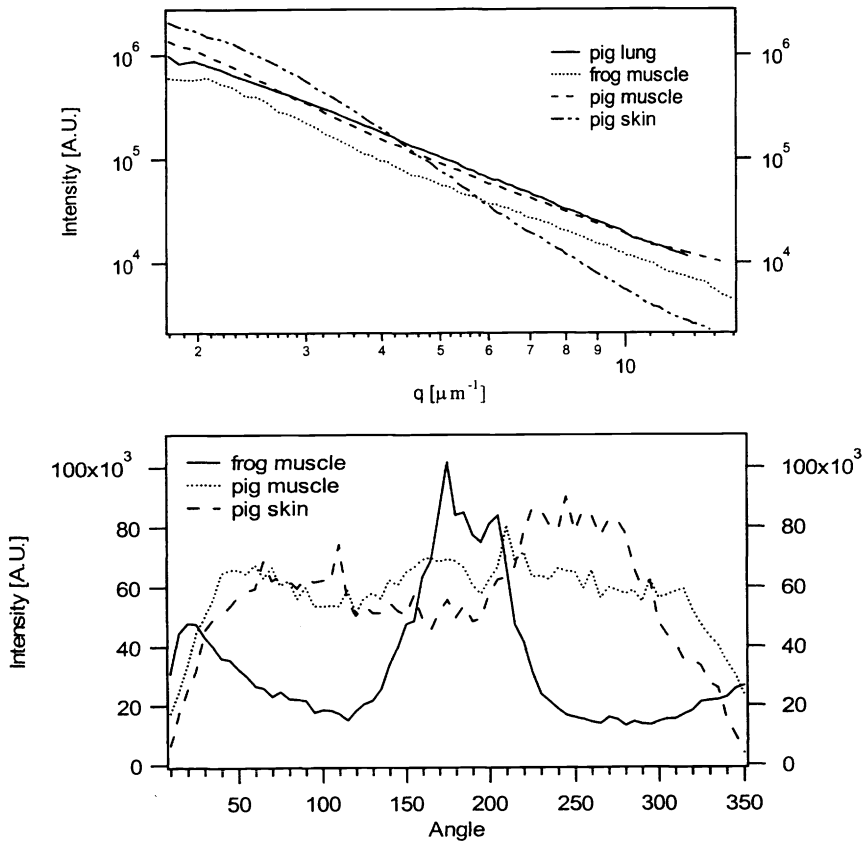

Figure 7: Averaged form factors and directional analysis for different tissues. The form factor decays with a power law coefficient of –3.7 for skin, whereas all other tissue types show a decay with a coefficient close to - 2.5. Averaging of all measurements of a Xenopus muscle sample under fixed orientation shows the almost constant direction of the muscle fibers throughout the sample. The porcine muscle average showed no preferred orientation of the fibers. The porcine skin sample showed a vague preferred direction, most probably due to the selection of spots.

4.CONCLUSIONS

In this report, we have shown our initial observations gained by applying the light scattering microscope to tissue. We set out to see whether and how to distinguish tissues on the basis of their light scattering patterns. This effort is motivated by the observation that a significant fraction of pathologists observations of tissue involve recognizing the presence and absence of structural order in tissue slices. We performed light scattering and imaging of multiple tissues, always looking at small (70 μm) spots from 20 μm slices. We observe significant differences due to super- and extra-cellular structures and heterogeneities in 20 μm thick tissue – these differences would not be systematically accessible without the scattering microscope.

Several strategies were employed to distinguish between scattering patterns. First, we analyze numerous measurements on randomly selected spots, to show how these single experiments contribute to average scattering. In this analysis, we look at the power law that describes the decay of the averaged form factors. We found, that skin is distinct from other tissues as its form factor decays with approximately $q^{-3.2}$ to $q^{-3.7}$ for wave vectors between $q = 2.7\mu m^{-1}$ and $q = 11.9\ \mu m^{-1}$. A possible explanation in terms of scattering from randomly oriented surfaces has been given. The same analysis does not segregate different types of similar tissues, striated porcine muscle sample and striated Xenopus Sartorius muscle, despite quite different structures -- the Xenopus muscle has well aligned muscle fibers parallel to the surface of the coverslip, whereas the (randomly sectioned) porcine muscle showed fibers of all different orientations. These organizational differences appear when the azimuthal dependence is analyzed.

Our technique is very useful for the detection and measurement of heterogeneities in tissues, as we have simultaneous microscopic information about the region where we perform our light scattering experiment. Measurements from a common heterogeneity in skin like a hair have been shown as example how a heterogeneity and the region around it can be measured in a scanning fashion revealing local ordering and anisotropies not previously accessible by scattering. We see clearly that with microscopic spatial resolution, tissues can not be treated as homogenous media and that large structures, ordering and anisotropy over tens of microns is responsible for a significant fraction of the total scattered light.

Using thin tissue slices as samples, we keep our investigation close to patho- histological studies. It is apparent that the scattering pattern contains a signature of local structure and organization [30, 36, 37]. Further development of the analysis of these scattering patterns may be useful for automatically detecting certain types of order. It is unlikely that light scattering without microscopy would be a reliable tool for pathology as the real-space image is needed to provide context for scattering measurement. In particular, the mode of operation is likely to be one in which a pathologist focusses on a suspicious region and collects a scattering pattern which can be analyzed quantitatively for relevant order and organization. Further development towards pathology requires focussed work on a particular problem of interest.

ACKNOWLEDGEMENTS

We are grateful to acknowledge the generous gift of excised frozen Xenopus Sartorius muscle from Pierre Tijskens (University of Pennsylvania). Furthermore, we'd like to thank David Boas (Massachusetts General Hospital) for the porcine tissue, Jia Quian Ren (Massachusetts General Hospital) for the possibility to use the cryomicrotome in his institute and Marge Lehman (Unilever Research) for preparing preliminary samples. This work was partially supported by a grant from Unilever Research.

REFERENCES

1. J. R. Mourant, I. J. Bigio, J. Boyer, R. L. Conn, T. Johnson, and T. Shimada, "Spectroscopic Diagnosis of bladder cancer with elastic light scattering," *Lasers in Surg. Med.* **17**, pp. 350-357, 1995.
2. J. B. Fishkin, O. Coquoz, E. R. Anderson, M. Brenner, and B. J. Tromberg, "Frequency-domain photon migration measurements of normal and malignant tissue optical properties in a human subject," *Appl. Optics* **36**, pp. 10-20, 1997.
3. V. V. Tuchin, "Light scattering study of tissues," *Physics- Uspekhi* **40**, pp. 494-515, 1997.
4. V. V. Tuchin, S. R. Utz, and I. V. Yaroslavsky, "Tissue Optics, Light-Distribution, and Spectroscopy," *Optical Engineering* **33**, pp. 3178-3188,.1994.
5. D. A. Boas and A. G. Yodh, "Spatially varying dynamical properties of turbid media probed with diffusing temporal light correlations," *JOSA A*, **14**, pp. 192-213, 1997.
6. S. J. Matcher, M. Cope, and D. T. Delpy, "*In vivo* measurements of the wavelength dependence of tissue-scattering coefficients between 760 and 900 nm measured with time-resolved spectroscopy," *Appl. Optics* **36**, pp. 386-396, 1997.
7. H. Liu, D. A. Boas, Y. Zhang, A. G. Yodh, and B. Chance, "Determination of optical properties and blood oxygenation in tissue using continuous NIR light," *Physics in Medicine & Biology* **40**, pp. 1983-93, 1995.
8. J. Laufer, R. Simpson, M. Kohl, M. Essenpreis, and M. Cope, "Effect of temperature on the optical properties of ex vivo human dermis and subdermis," *Phys. Med. Biol.* **43**, pp. 2479-2489, 1998.
9. J. B. Dawson, D. J. Barker, D. J. Ellis, E. Grassam, J. A. Cotterill, G. W. Fisher, and J. W. Feather, "A theoretical and experimental study of light absorption and scattering by in vivo skin," *Phys. Med. Biol.* **25**, pp. 695-709, 1980.
10. A. Wiel, G. Bruls, and C. v. d. Leun, "Forward scattering properties of human epidermal layers," *Photochem. Photobiol.* **40**, pp. 231-242, 1984.
11. S. P. Treweek and J. C. Barbenel, "Direct measurement of the optical properties of human breast skin," *Med. Biol. End. & Comput*, **34**, pp. 285-289, 1996.
12. S. L. Jacques, C. A. Alter, and S. A. Prahl, "Angular dependence of HeNe laser light scattering by human dermis," *Lasers in Life Sc.* **1**, pp. 309-333, 1987.
13. D. A. Boas, M. A. O'Leary, B. Chance, and A. G. Yodh, "Scattering of diffuse photon density waves by spherical inhomogeneities within turbid media: analytic solution and applications," *Proceedings of the National Academy of Sciences of the United States of America* **91**, pp. 4887-91, 1994.
14. M. A. O'Leary, D. A. Boas, B. Chance, and A. G. Yodh, "Experimental Images of Heterogeneous Turbid Media By Frequency- Domain Diffusing-Photon Tomography," *Optics Letters* **20**, pp. 426-428, 1995.
15. E. M. Sevick, C. L. Burch, and B. Chance, "Near-infrared optical imaging of tissue phantoms with measurement in the change of optical path lengths," *Advances in Experimental Medicine & Biology* **345**, pp. 815-823, 1994.

16. W.-F. Cheung, S. A. Prahl, and A. J. Welch, "A review of the optical properties of biological tissues," *IEEE J. Quantum Electron.* **26**, pp. 2166-85, 1990.
17. J. R. Mourant, J. P. Freyer, A. H. Hielscher, A. A. Eick, D. Shen, and T. M. Johnson, "Mechanisms of light scattering from biological cells relevant to noninvasive optical- tissue diagnostics," *Appl. Optics* **37**, pp. 3586-3593, 1998.
18. R. Drezek, A. Dunn, and R. Richards-Kortum, "Light scattering from cells: finite difference time domain simulations and goniometric measurements," *Applied Optics* **38**, pp. 3651-3661, 1999.
19. B. Beauvoit, H. Liu, K. Kang, P. D. Kaplan, M. Miwa, and B. Chance, "Characterization of absorption and scattering properties for various yeast strains by time-resolved spectrscopy," *Cell Biophys.* **23**, pp. 91-109, 1993.
20. B. Beauvoit and B. Chance, "Time-resolved spectroscopy of mitochondria, cells, and tissues under normal and pathological conditions," *Mol. Cell. Biochem.* **184**, pp. 445-455, 1998.
21. M. J. C. Van Gemert, S. L. Jacques, H. J. C. M. Sterenborg, and W. M. Star, "Skin optics," *IEEE Transactions on Biomedical Engineering* **36**, pp. 1146-54, 1989.
22. J. F. Beek, P. Blokland, P. Posthumus, M. Aalders, J. W. Pickering, H. J. C. M. Sterenborg, and M. J. C. v. Gemert, "*In vi*tro double-intergrating sphere optical properties of tissues between 630 and 1064 nm," *Phys. Med. Biol.* **42**, pp. 2255-2261, 1997
23. A. H. Hielscher, R. E. Alcouffe, and R. L. Barbour, "Comparism of finite- difference transport and diffusion calculations for photon migration in homogenous and heterogenous tissues," *Phys.Med.Biol.* **43**, pp. 1285-1302, 1998.
24. S. R. Arridge, M. Cope, and D. T. Delpy, "The theoretical basis for the determination of optical pathlengths in tissue: temporal and frequency analysis," *Phys.Med.Biol.* **37**, pp. 1531-1560, 1992
25. D. J. Smithies and P. H. Butler, "Modeling the distribution of laser light in port-wine stains with the Monte- Carlo method," *Phys.Med.Biol.* **40**, pp. 701-731, 1995
26. G. Videen and D. Ngo, "Light scattering multipole solution for a cell," *J.Biomed.Opt.* **3**, pp. 212-220, 1998.
27. J. M. Schmitt and G. Kumar, "Optical Scattering properties of soft tissue: a discrete model," *Appl. Optics* **37**, pp. 2788-2797, 1998.
28. P. D. Kaplan, V. Trappe, and D. A. Weitz, "Light Scattering Microscope," *Appl. Optics* **38**, pp. 4151-4157, 1999.
29. T. Maeda and S. Fujime, "Quasielastic light scattering under optical microscope," *Rev. Sci. Instr.* **43**, pp. 566-567, 1972.
30. I. Nishio, T. Tanaka, S.-T. Sun, Y. Imanishi, and S. T. Ohnishi, "Hemoglobin aggregation in single red blood cells of sickle cell anemia," *Science* **220**, pp. 1173-1174, 1983.
31. I. Nishio, J. Peetermans, and T. Tanaka, "Microscope laser light scattering spectroscopy of single biological cells," *Cell Biophys.* **7**, pp. 91-105, 1985.
32. P. S. Blank, R. B. Tishler, and F. D. Carlson, "Quasielastic light scattering microscope spectrometer," *Appl. Optics.* **26**, pp. 351, 1987.
33. L. P. Gartner and J. L. Hiatt, *Color Textbook of Histology*. Philadelphia: W.B. Saunders Company, 1997.
34. L. T. Perelman, V. Backman, M. Wallace, G. Zonios, R. Manoharan, A. Nusrat, S. Shields, M. Seiler, C. Lima, T. Hamano, I. Itzkan, J. VanDam, J. M. Crawford, and M. S. Feld, "Observation of periodic fine structure in reflectance from biological tissue: A new technique for measuring nuclear size distribution," *Physical Review Letters* **80**, pp. 627-630, 1998.
35. B. A. Fedorov, B. B. Fedorovov, and P. W. Schmidt, "An analysis of the fractal properties of the surface of globular proteins," *J. Chem. Phys.* **99**, pp. 4076-4084, 1993.
36. J. A. Peetermans, B. D. Foy, and T. Tanaka, "Accumulation and diffusion of crystallin inside single fiber cells in intact chicken embryo lenses," *Proc. Natl. Acad. Sci.* **84**, pp. 1727-1730, 1987.
37. J. A. Peetermans, E. K. Matthews, I. Nishio, and T. Tanaka, "Particle motion in single acinar cells observed by microscope laser light scattering spectroscopy," *Eur. Biophys. J.* **15**, pp. 65-69, 1987.